

Single Pt Atoms Confined into a Metal–Organic Framework for Efficient Photocatalysis

Xinzuo Fang, Qichao Shang, Yu Wang, Long Jiao, Tao Yao, Yafei Li, Qun Zhang, Yi Luo, and Hai-Long Jiang*

It is highly desirable yet remains challenging to improve the dispersion and usage of noble metal cocatalysts, beneficial to charge transfer in photocatalysis. Herein, for the first time, single Pt atoms are successfully confined into a metal–organic framework (MOF), in which electrons transfer from the MOF photosensitizer to the Pt acceptor for hydrogen production by water splitting under visible-light irradiation. Remarkably, the single Pt atoms exhibit a superb activity, giving a turnover frequency of 35 h^{-1} , ≈ 30 times that of Pt nanoparticles stabilized by the same MOF. Ultrafast transient absorption spectroscopy further unveils that the single Pt atoms confined into the MOF provide highly efficient electron transfer channels and density functional theory calculations indicate that the introduction of single Pt atoms into the MOF improves the hydrogen binding energy, thus greatly boosting the photocatalytic H_2 production activity.

Unfortunately, given the high surface energy, single atoms are typically mobile and prone to aggregation.^[2] The fabrication of single atom catalysts that are stable during catalytic reaction remains a significant challenge. To this end, the key point is to develop suitable supports that possess strong interaction with the single metal atoms. So far, metal oxides and some porous materials (e.g., zeolites and carbon-based materials) have been demonstrated to be good candidates to stabilize single atoms.^[1,3] The defects,^[1a,d,e] voids,^[1f,g] and particularly coordinatively unsaturated sites^[3a] in the support materials are very important to anchor individual metal atoms and maintain the high dispersion of single atoms.

Single-atom catalysts, as a new class of promising catalysts featuring atomically dispersed metal atoms anchored on supports, have drawn increasing attention.^[1–3] With maximized atomic efficiency, single atom catalysts have shown excellent catalytic performance toward diverse reactions, including oxidation, hydrogenation, water-gas shift, electrocatalysis, etc.

Alternatively, a relatively new class of porous crystalline materials, metal–organic frameworks (MOFs), which have a lot of potential coordination sites, defects, and porosities to anchor metal atoms, might be ideal supports to stabilize single atoms for catalysis.^[4] MOFs have been demonstrated to be excellent stabilizers for metal nanoparticles (NPs) and show their synergistic catalysis.^[5] Differently from the inorganic supports with single atoms or metal NPs stabilized on their surfaces only, the MOF pores afford spaces for additional metal atoms introduced and would prevent them from aggregation. The metal-oxo clusters in MOFs can behave as oxygen-donor ligands to connect additional metal ions.^[6] The emerging structural defects in MOFs also create new sites to anchor the single metal atoms.^[4e] More importantly, MOFs are able to provide affluent potential coordination sites ready for implanting single metal atoms by selecting suitable organic struts or via postsynthetic modification of functionalized bridging linkers.^[7] Similarly to the intercalation of single metal atoms into the characteristic N-coordinating cavities in porous polymeric C_3N_4 ,^[1d,3b] the porphyrin struts in MOFs involving four pyrrolic nitrogen sites in a square-planar geometry are very promising and offer inherent conditions to firmly trap single metal atoms. Therefore, porphyrinic MOFs might be ideal scaffolds for the intercalation of single metal atoms.^[7c–e] Despite the great opportunity described above, unfortunately, to the best of our knowledge, single metal atom hosted by MOFs has never been reported thus far.


Herein, we demonstrate for the first time that MOFs are a class of promising supports/hosts to stabilize single metal atoms for efficient catalysis. A highly stable aluminum-based porphyrinic MOF, formulated as $(\text{AlOH})_2\text{H}_2\text{T CPP}$ ($\text{H}_2\text{T CPP} = 4,4',4'',4'''$ -(porphyrin-5,10,15,20-tetrayl)tetrabenzoate)^[7c] denoted

X. Fang, L. Jiao, Prof. H.-L. Jiang
Hefei National Laboratory for Physical Sciences at the Microscale
CAS Key Laboratory of Soft Matter Chemistry
Collaborative Innovation Center of Suzhou
Nano Science and Technology
Department of Chemistry
University of Science and Technology of China
Hefei, Anhui 230026, P. R. China
E-mail: jianglab@ustc.edu.cn

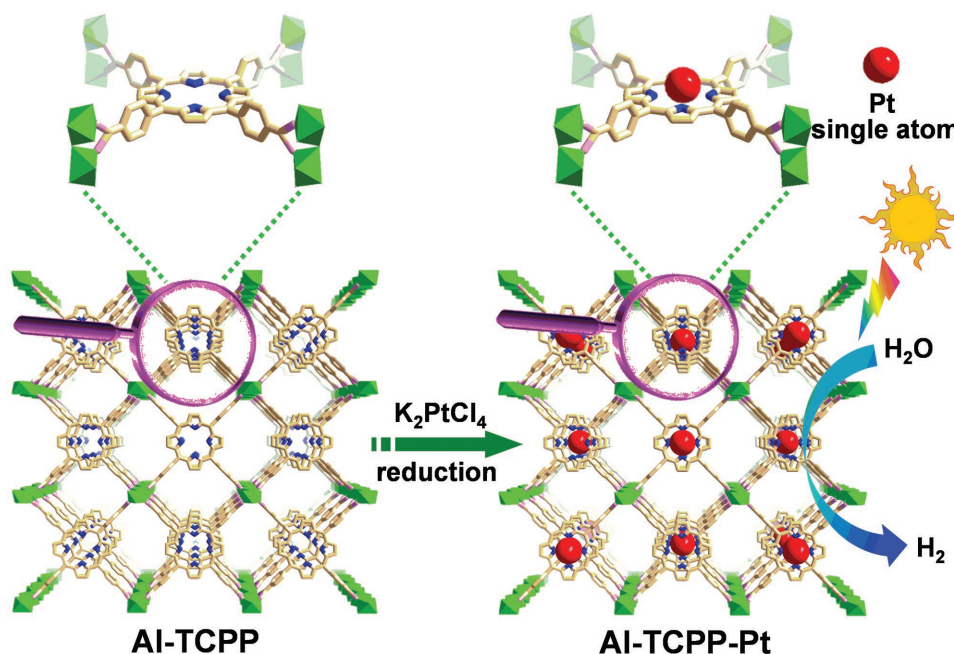
Q. Shang, Prof. Q. Zhang, Prof. Y. Luo
Hefei National Laboratory for Physical Sciences at the Microscale
Synergetic Innovation Center of Quantum Information
and Quantum Physics
Department of Chemical Physics
University of Science and Technology of China
Hefei, Anhui 230026, P. R. China

Y. Wang, Prof. Y. Li
College of Chemistry and Materials Science
Nanjing Normal University
Nanjing 210023, China

Prof. T. Yao
National Synchrotron Radiation Laboratory
University of Science and Technology of China
Hefei, Anhui 230026, P. R. China

 The ORCID identification number(s) for the author(s) of this article can be found under <https://doi.org/10.1002/adma.201705112>.

DOI: 10.1002/adma.201705112



Scheme 1. Schematic illustration showing the synthesis of Al-TCPP-Pt for photocatalytic hydrogen production.

as Al-TCPP, in which infinite $\text{Al}(\text{OH})\text{O}_4$ chains are interconnected by the porphyrin linkers into a 3D microporous framework, was employed for Pt(II) metalation into the porphyrin centers. Following a simple reduction, we obtained single Pt atoms based on the strong interaction with pyrrolic N atoms in the Al-TCPP (**Scheme 1**). The spherical aberration-corrected electron microscope observation and X-ray adsorption fine structure (XAFS) results unambiguously evidenced the presence of single Pt atoms inside the MOF. Remarkably, the resultant MOF incorporating with single Pt atoms (denoted Al-TCPP-Pt hereafter) exhibits an extremely high photocatalytic hydrogen production rate by water splitting, far superior to that of the reference catalyst, Pt NPs stabilized by Al-TCPP, under visible-light irradiation, thanks to the maximized Pt utilization in the former. In addition, ultrafast transient absorption (TA) spectroscopy characterization has been performed to reveal the involved mechanism for photocatalysis, that is, the single Pt atoms provide highly efficient electron transfer channels and hence greatly boost the photocatalytic activity. The density functional theory (DFT) calculations further reveal that the introduction of single Pt atoms into Al-TCPP not only contributes to the density of states near Fermi level but also improves the hydrogen binding energy.

The Al-TCPP was synthesized by the hydrothermal reaction of $\text{AlCl}_3 \cdot 6\text{H}_2\text{O}$ and H_2TCPP at 180°C . The Pt(II) ions were implanted into the center of porphyrin linkers in Al-TCPP through a simple liquid-phase reaction between Al-TCPP and K_2PtCl_4 to yield Al-TCPP-Pt(II), which was reduced at 180°C in H_2 atmosphere to obtain single Pt atoms inside Al-TCPP. The Pt contents are adjustable according to the loading amount of K_2PtCl_4 (Table S1, Supporting Information), and the obtained catalysts with Pt loadings of 0.07 and 0.29 wt% are denoted Al-TCPP-0.1Pt and Al-TCPP-0.3Pt, respectively.

The negligible difference between the X-ray diffraction patterns of Al-TCPP and Al-TCPP-Pt indicates that the introduction of Pt does not bring about any influence on the crystallinity and structure of Al-TCPP (Figure S1, Supporting Information). N_2 sorption isotherms further indicate the porous structure can be well retained after Pt introduction (Figure S2, Supporting Information). Transmission electron microscopy (TEM) image does not exhibit observable particles (**Figure 1a**), probably due to the resolution limit of TEM. Delightedly, the existence of abundant Pt single atoms can be evidenced by aberration-corrected high-angle annular dark-field scanning transmission electron microscopy (HAADF-STEM), which is a very powerful tool to discern individual heavy atoms in a localized area. As shown in Figure 1b, the bright spots in Al-TCPP-0.1Pt correspond to single Pt atoms with ultrasmall sizes between 0.1 and 0.2 nm uniformly dispersed inside Al-TCPP (Figure 1b, inset). The intensity profile also indicates isolated Pt atoms separated by ≈ 0.5 nm (Figure 1c). Although there is still no obvious particle in the TEM image of Al-TCPP-0.3Pt (Figure S3, Supporting Information), the aberration-corrected HAADF-STEM image clearly shows the presence of single Pt atoms and a little bit Pt clusters together (Figure S4, Supporting Information), indicating that slight Pt aggregation occurs with increasing Pt content.

Given that electron microscope generally provides structural information for specific local area only, XAFS analysis has been conducted to further acquire more overall structural information on atomic distribution. X-ray absorption near-edge structure (XANES) analysis was first carried out to observe the electronic structure of Pt. It can be found that the white line peak corresponding to an electronic transition from $2p_{2/3}$ to unoccupied 5d states displays an obviously high intensity for Al-TCPP-0.1Pt, implying a more oxidized electronic structure of Pt.^[1a,3c] It can be seen that the white-line intensity of Al-TCPP-0.1Pt is much

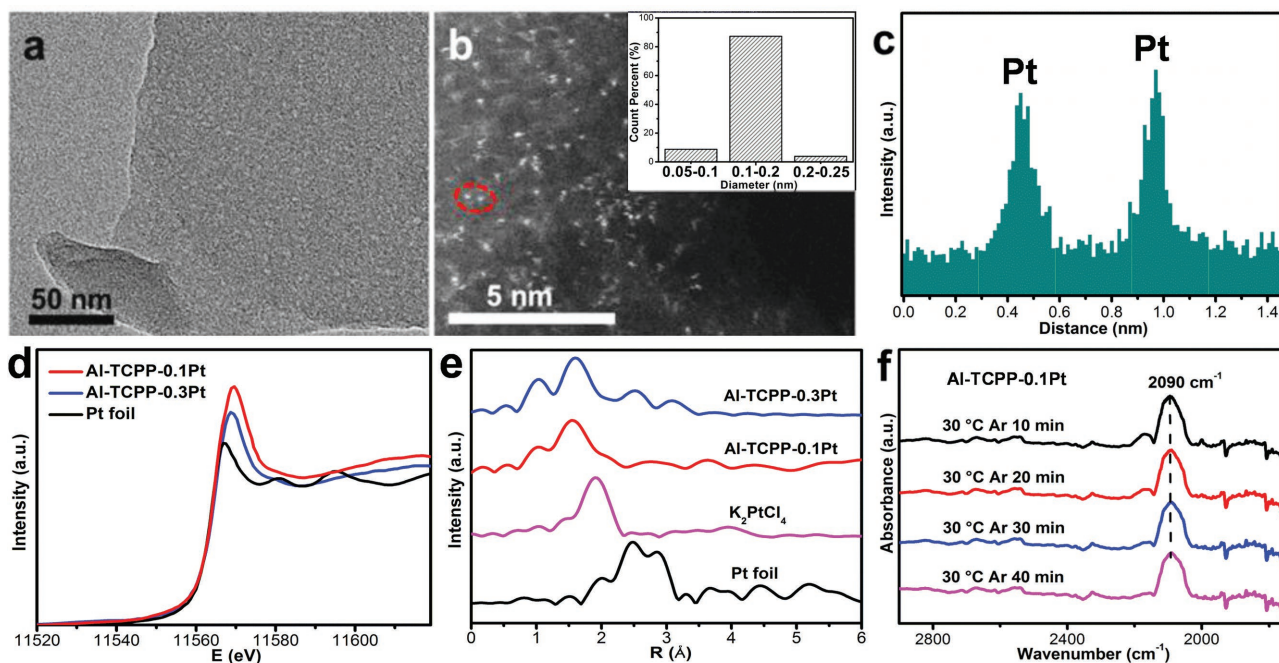


Figure 1. a) TEM and b) aberration-corrected HAADF-STEM images of Al-TCPP-0.1Pt, c) line-scanning intensity profile obtained from the area highlighted with red circle in (b). d) The normalized XANES spectra at the Pt L_3 -edge of Al-TCPP-0.3Pt, Al-TCPP-0.1Pt, and Pt foil. e) Fourier transformed (FT) k^3 -weighted $\chi(k)$ -function of the EXAFS spectra for Al-TCPP-0.3Pt, Al-TCPP-0.1Pt, K_2PtCl_4 , and Pt foil. f) DRIFT spectra of CO adsorbed on Al-TCPP-0.1Pt after being purged with Ar gas for different time lengths.

higher than that of Pt foil (Figure 1d), indicating that Pt species is in the oxidized forms (Pt^{2+}) in Al-TCPP-0.1Pt. In contrast, the slightly lower white-line intensity of Al-TCPP-0.3Pt clearly shows the lower valence states of Pt in Al-TCPP-0.3Pt than that in Al-TCPP-0.1Pt.^[1a,e] To obtain more information on the local structure of Pt, the extended X-ray absorption fine structure (EXAFS) spectra have been further performed. It shows that there is one prominent peak at ≈ 1.5 Å from the Pt-N contribution with the absence of significant Pt-Cl (≈ 1.9 Å) or Pt-Pt (≈ 2.7 Å) bond in Al-TCPP-0.1Pt (Figure 1e), confirming that the single-atom Pt has been stabilized by nitrogen atoms and almost no (or very few) Pt particles or clusters exist in Al-TCPP-0.1Pt. This can be further proved by basically only the Pt-N peak in the fitting result (Table S2, Supporting Information) and is also in good agreement with the above HAADF-STEM result (Figure 1b and Figure S5, Supporting Information).^[1a,e] As the weight percentage of Pt increases, the structural feature changes dramatically. It can be seen that the Al-TCPP-0.3Pt presents two evident peaks at around 1.5 and 2.7 Å, suggesting the coexistence of single-atom Pt and Pt clusters (Figure 1e and Figure S6, Supporting Information), which also explains the lower valence states of Pt in Al-TCPP-0.3Pt than that in Al-TCPP-0.1Pt mentioned above. The carbon monoxide (CO) adsorption behavior of Al-TCPP-0.1Pt was also investigated using diffuse reflectance infrared Fourier transform (DRIFT) spectroscopy. Generally, infrared spectroscopy using CO as the probe molecule is a fast and convenient characterization method to directly identify single atoms from nanoparticles. It is a nonlocal characterization compared with HAADF-STEM and provides solid evidence for the formation of single Pt atoms. In our DRIFTS measurements for Al-TCPP-0.1Pt, upon purging with Ar to remove any

loosely adsorbed species (gaseous CO), only a peak centered at 2090 cm^{-1} was observed, which was assigned to CO chemisorbed on single Pt atoms (Figure 1f). The symmetric property of the peak indicates the uniform structure of the single Pt atom, which is similar to previous reports.^[1i,2d] As we expected, no band appears in the range $2080\text{--}2030$ and $1920\text{--}1950\text{ cm}^{-1}$ assignable to the linear- and bridged-adsorbed CO on Pt clusters and NPs, implying that all Pt species would be atomically dispersed.^[1a] More importantly, the CO chemisorption peak remains intact during the Ar purge, which suggests a lack of interaction between adsorbed CO molecules (so called dipole-dipole coupling correlation) and further confirms the existence of single Pt atoms.

For comparison, Pt NPs of ≈ 3 nm stabilized by Al-TCPP (denoted Al-TCPP-PtNPs) were also synthesized (Figures S7 and S8, Supporting Information). The optical properties were first evaluated using UV-vis absorption spectra (Figure 2a). The Al-TCPP shows a broad and strong absorption in the region of $200\text{--}800$ nm due to the feature of the porphyrin ligand. The introduction of single Pt atoms or Pt NPs into the MOF does not cause significant change in the absorption spectra, revealing their similar light absorption behavior. Photoluminescence (PL) spectra for Al-TCPP-0.1Pt and Al-TCPP-PtNPs as well as the pristine Al-TCPP were measured under excitation at 400 nm (Figure 2b). The steady-state PL spectra show that the two PL bands centered at ≈ 650 and 750 nm are strong for Al-TCPP, while they become much weaker for Al-TCPP-PtNPs and the weakest for Al-TCPP-0.1Pt. The obvious PL quenching indicates rapid electron transfer from Al-TCPP to Pt NPs and the most efficient electron transfer can be achieved in the presence of single Pt atoms. Photocurrent measurements unveil

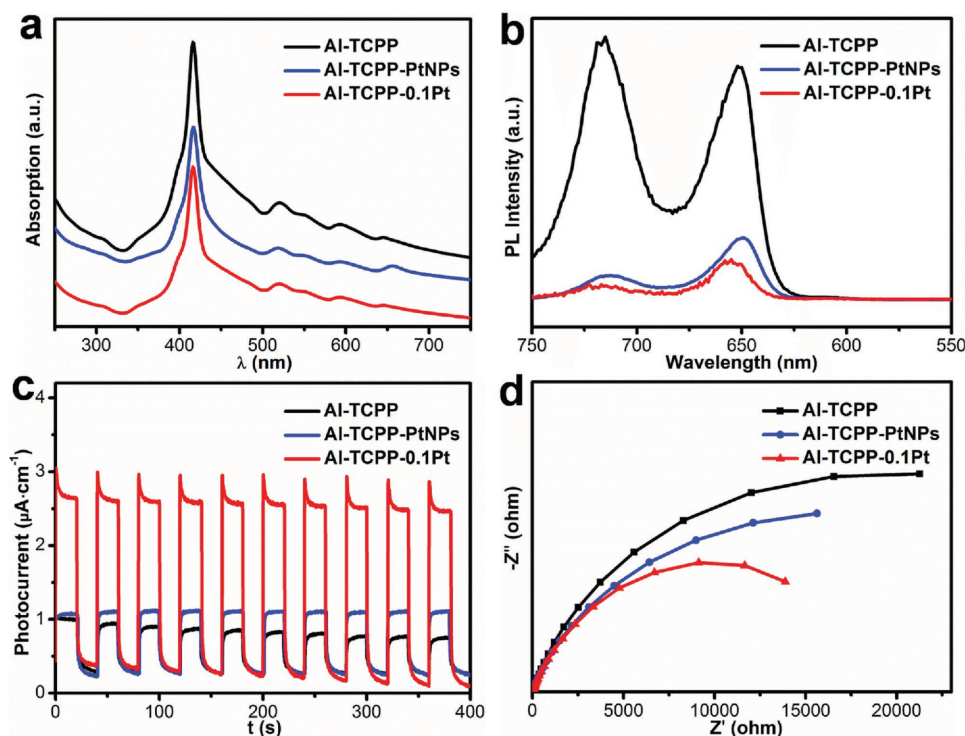


Figure 2. a) UV-vis spectra, b) photoluminescence emission spectra, c) photocurrent responses, and d) EIS Nyquist plots for Al-TCPP, Al-TCPP-PtNPs, and Al-TCPP-0.1Pt.

the charge-separation efficiency of catalysts and agree with the PL results. As expected, Al-TCPP-0.1Pt possesses the strongest photocurrent response among all samples (Figure 2c), indicating that the recombination of photogenerated electrons and holes is mostly inhibited and the best charge transfer from Al-TCPP to single Pt atoms under visible-light irradiation. The results can be further supported by electrochemical impedance spectroscopy (EIS) investigations, in which Al-TCPP-0.1Pt exhibits the smallest resistance, reflecting its fastest interfacial charge transfer between Al-TCPP-0.1Pt and medium (Figure 2d).

Encouraged by the above characterization results, we further examined the photocatalytic H₂ production by water splitting, using triethanolamine as sacrificial agent and CH₃CN

as solvent under visible-light irradiation. As demonstrated in previous reports on MOF photocatalysis,^[8] the organic linkers with π conjugation as light harvester can be photoexcited transfer energy to M-oxo clusters via linker-to-cluster charge transfer mechanism. The electrons can be then transferred to the cocatalyst for reduction reaction. In our system, as the Al-oxo chains cannot accept electrons from the porphyrin linker, the photogenerated electrons would be directly transferred to the Pt cocatalyst. As displayed in Figure 3a, even if Al-TCPP exhibits strong visible-light absorption, it shows a negligible activity of 1.5 $\mu\text{mol g}^{-1} \text{h}^{-1}$ possibly due to the fast electron-hole recombination. When Pt NPs are introduced, the Pt with a low overpotential is able to trap electrons and behaves as proton reduction sites. As a result, Al-TCPP-PtNPs

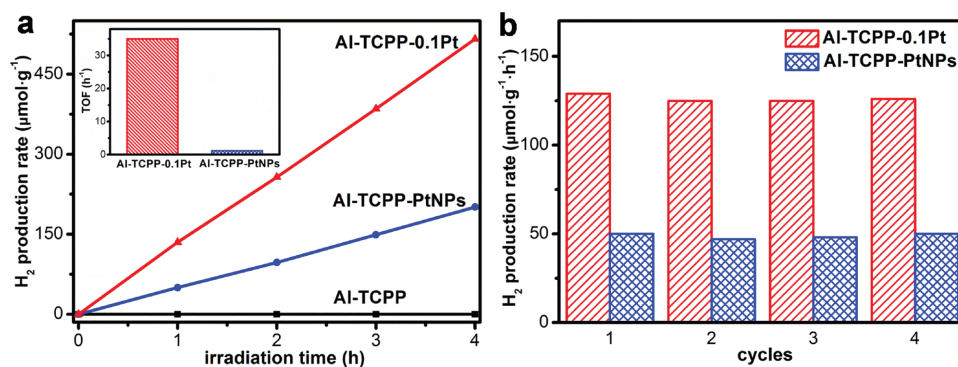


Figure 3. a) Photocatalytic hydrogen production rates of Al-TCPP, Al-TCPP-PtNPs, and Al-TCPP-0.1Pt (inset: the calculated TOFs of Al-TCPP-PtNPs and Al-TCPP-0.1Pt). b) Recycling performance comparison for Al-TCPP-PtNPs and Al-TCPP-0.1Pt.

exhibits a much higher photocatalytic H₂ production rate of 50 μmol g⁻¹ h⁻¹. Delightedly, downsizing the Pt into single atoms, Al-TCPP-0.1Pt exhibits the best photocatalytic efficiency of 129 μmol g⁻¹ h⁻¹. Significantly, the calculated turnover frequency (TOF) of Al-TCPP-0.1Pt reaches 35 h⁻¹, ≈30 times that of 1.1 h⁻¹ for Al-TCPP-PtNPs (Figure 3a, inset). Such a TOF value is higher than that of almost all previously reported Pt-MOF photocatalysts and even comparable to Pt/semiconductor photocatalysts (Tables S3 and S4, Supporting Information). The result unambiguously demonstrates that single-atom Pt cocatalyst with the maximized atomic utilization drastically boosts the photocatalytic activity even at a very low Pt content. In contrast, Al-TCPP-0.1Pt(II) without subsequent reduction displays negligible photocatalytic H₂ production, further indicating that the reduction of Pt(II) to single Pt atoms are crucial to the significant activity (Figure S9, Supporting Information). The control sample TCPP-0.1Pt obtained in a similar method to that of Al-TCPP-0.1Pt also exhibits poor activity toward H₂ production (Figure S10, Supporting Information), manifesting that the introduction of TCPP into MOFs realizes the significant enhancement of photocatalytic performance. Accordingly, the photocatalytic activity is further improved as the Pt loading increases. The Al-TCPP-0.3Pt exhibits a higher rate of 181 μmol g⁻¹ h⁻¹, whereas its TOF only reaches 11.8 h⁻¹ due to its low atom efficiency of Pt clusters, which has been confirmed previously (Figures 1d,e and Figure S11, Supporting Information). The stability of the samples has been verified by recycling experiments. Both samples demonstrate no noticeable change in the hydrogen-production rate during the four catalytic runs (Figure 3b). The powder X-ray diffraction after catalytic recycles supports the well-retained crystallinity and structural integrity of both catalysts, suggesting their high stability under photocatalytic conditions (Figure S12, Supporting Information). Given the mobility of single atoms, we further confirmed the stability of Pt single atoms by TEM and HAADF-STEM observation. Delightedly, no particle observed in the TEM and HAADF-STEM images reveals that the Pt still remains the form of isolated atoms in Al-TCPP without aggregation (Figures S13 and S14, Supporting Information). Combined with recycling experiments in the photocatalytic process, these results well demonstrate the stability of single-atom Pt cocatalyst in Al-TCPP.

The information above highlighted the niche of stabilizing Pt single atoms by Al-TCPP for the photocatalytic activity enhancement. As the catalysis is grounded on a charge-transfer event following photoexcitation, it is essential to gain insights into the mechanism involved. Therefore we resorted to a robust tool, ultrafast TA spectroscopy,^[9] to track in real time the charge carrier dynamics in these nanocomposites. In the TA measurements, we adopted a pump-probe configuration with femtosecond UV pump and white-light-continuum probe (see Section S1, Supporting Information). The pump laser was chosen at 400 nm (center wavelength), which can effectively excite the samples (refer to the UV-vis spectra in Figure 2a). Since the registered TA kinetic profiles show no essential variation at different probing wavelengths within 520–640 nm, we here show a representative set of data taken at 540 nm (Figure 4). For pristine Al-TCPP, following a positive-value excited-state absorption signal after photoexcitation, it features an extremely long recovery (with a dominant ultraslow decay component $\tau \gg 4$ ns). On the basis

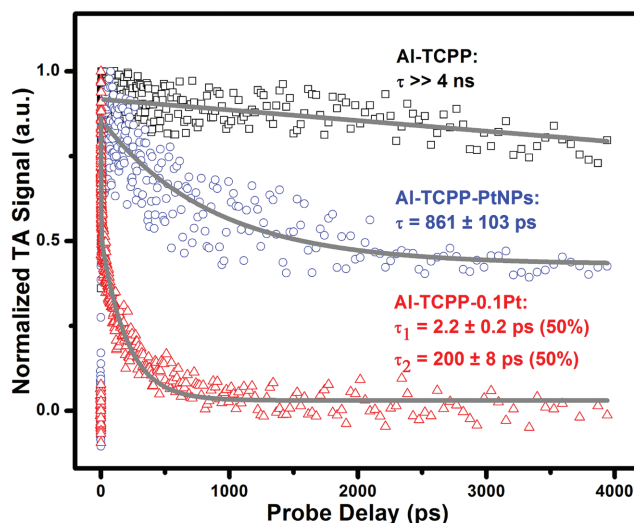


Figure 4. Comparison of the ultrafast TA kinetics (pump at 400 nm and probe at 540 nm) for Al-TCPP, Al-TCPP-PtNPs, and Al-TCPP-0.1Pt.

of the previous observations in typical MOFs,^[10] this slow decay process can be ascribed to a long-lived intermediate state, where the photoexcited electrons get trapped and can hardly be utilized for the redox reaction in solvent. In stark contrast, Al-TCPP-PtNPs exhibits an obvious acceleration of the TA kinetics, featuring a shorter, dominant time constant $\tau = 861 \pm 103$ ps. Similarly to the previous reports on other nanocomposites,^[11] the incorporation of noble metal into MOFs can bring about an additional electron-transfer channel and the observed acceleration should be attributed to this channel opening. The electron-transfer channel from Al-TCPP to Pt realizes the spatial separation of photoexcited charge carriers, thereby suppressing the detrimental electron-hole combination therein. More importantly, it turns out that the loading of single atoms leads to a much pronounced acceleration. The biexponential fitting results for Al-TCPP-0.1Pt are $\tau_1 = 2.2 \pm 0.2$ (50%) and $\tau_2 = 200 \pm 8$ ps (50%), with an average relaxation lifetime of 198 ± 8 ps, dramatically shortening the lifetime of Al-TCPP-PtNPs by more than fourfold. Clearly, downsizing Pt NPs into single atoms achieves stronger interaction between Al-TCPP and the noble metal, and hence results in greatly enhanced charge separation, which definitely benefits the catalytic performance.

The above experimental results demonstrate that the small content of single Pt atom leads to significantly enhanced photocatalytic H₂ production. We further performed DFT-based first-principles calculations to gain the fundamental insight into the role of single Pt atom in Al-TCPP-0.1Pt (see Section S3, Supporting Information). According to the density of states analysis (Figure S15, Supporting Information), Al-TCPP and Al-TCPP-0.1Pt possess nearly identical band gap and similar electronic states near the Fermi level, implying that they would show similar light absorption behavior, which is consistent with experimental findings; moreover, the single Pt atom in Al-TCPP-0.1Pt contributes to the states of valence band. Remarkably, Al-TCPP-0.1Pt exhibits significantly improved H binding free energy (ΔG_{H^*}) after the separation of electron and hole. As shown in the Figure 5a, the hole-involved Al-TCPP-0.1Pt (Figure 5b)

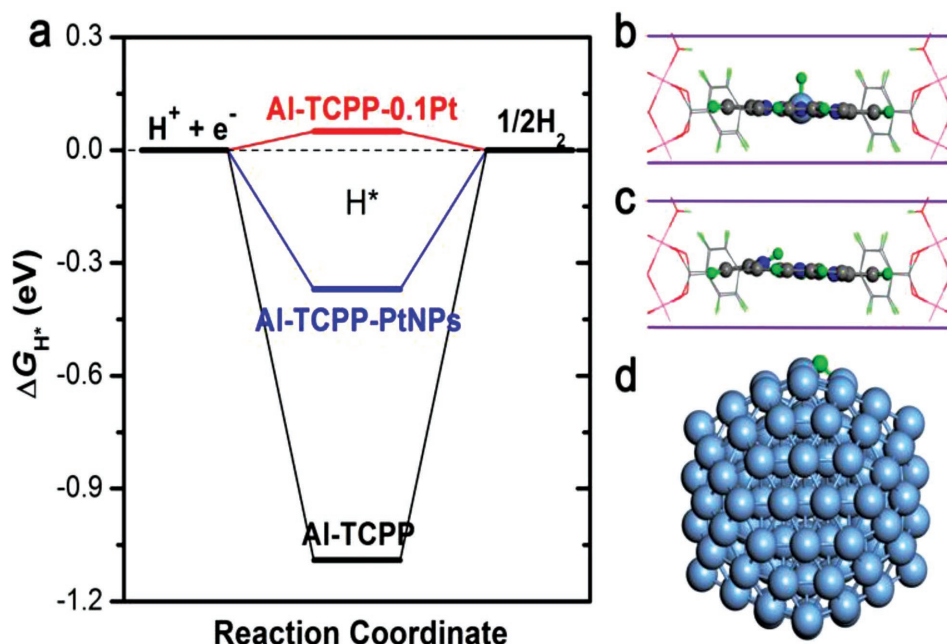


Figure 5. a) Calculated free energy diagram for photocatalytic H_2 production. Geometric structures of H^* of b) Al-TCPP-0.1Pt, c) Al-TCPP, and d) Al-TCPP-PtNPs (Pt_{147}). The sky-blue, grey, red, blue, pink, and green balls represent Pt, C, O, N, Al, and H atoms, respectively.

has a very appealing ΔG_{H^*} of 0.05 eV, which would guarantee both efficient electron-proton acceptance to form H^* and fast hydrogen desorption. In comparison, the ΔG_{H^*} of Al-TCPP-PtNPs (modeled with Pt_{147} cluster, Figure 5d) and hole-involved Al-TCPP (Figure 5c) are identified to be -0.37 and -1.09 eV, respectively, indicating strong hydrogen adsorptions and unfavorable hydrogen releases. Therefore, the superior photocatalytic activity of Al-TCPP-0.1Pt toward hydrogen production might be due to the effect of single Pt atom on optimizing H binding and electronic properties, followed by Al-TCPP-PtNPs and Al-TCPP, in good agreement with experimental results.

In conclusion, we have developed a facile synthetic strategy to atomically dispersed Pt into an MOF, which was well demonstrated by spherical aberration-corrected electron microscope observation and XAFS results. Significantly, given that the single Pt atoms maximize the atom utilization, the Al-TCPP-0.1Pt catalyst exhibits superb visible-light photocatalytic efficiency in hydrogen production. The achieved TOF value is ≈ 30 times than that of Pt NPs (≈ 3 nm) stabilized by Al-TCPP as well as that of all previously reported Pt-MOF composites on a per-Pt-atom basis. Spectroscopic characterizations and DFT calculations revealed that the introduction of single Pt atoms into Al-TCPP opens a highly efficient electron transfer channel and improves the hydrogen binding energy, which lead to significantly enhanced activity of H_2 production. The current study highlights the great potential and advantages in the formation of metal single-atom catalysts based on MOF systems. This work not only opens an avenue to the synthesis of single metal atoms stabilized by MOFs and provides a deep understanding of the electron-transfer mechanism for single metal atoms involved in MOFs but also stimulates further studies toward developing more efficient visible-light-responsive MOFs for photocatalysis utilizing solar energy.

Supporting Information

Supporting Information is available from the Wiley Online Library or from the author.

Acknowledgements

X.F., Q.S., and Y.W. contributed equally to this work. This work was supported by the National Natural Science Foundation of China (NSFC) (21725101, 21371162, 21673213, 21521001, 21573211, and 21633007), the National Research Fund for Fundamental Key Project (2014CB931803), the National Key R&D Program on Nano Science and Technology (2016YFA0200602), the Recruitment Program of Global Youth Experts, and the Fundamental Research Funds for the Central Universities of China (WK2340000063). The authors would like to thank Y. Pei at Iowa State University for XAFS data fitting, H. Wang at University of Science and Technology of China (USTC) for CO-DRIFTS measurement and thank Beijing Synchrotron Radiation Facility (BSRF) (Beamline 1W1B) and Shanghai Synchrotron Radiation Facility (SSRF) for the synchrotron beam time.

Conflict of Interest

The authors declare no conflict of interest.

Keywords

DFT calculation, metal-organic frameworks, photocatalysis, photocatalytic H_2 production, single atoms

Received: September 6, 2017

Revised: November 5, 2017

Published online: January 8, 2018

- [1] a) B. Qiao, A. Wang, X. Yang, L. F. Allard, Z. Jiang, Y. Cui, J. Liu, J. Li, T. Zhang, *Nat. Chem.* **2011**, *3*, 634; b) X.-F. Yang, A. Wang, B. Qiao, J. Li, J. Liu, T. Zhang, *Acc. Chem. Res.* **2013**, *46*, 1740; c) S. Liang, C. Hao, Y. Shi, *ChemCatChem* **2015**, *7*, 2559; d) X. Li, W. Bi, L. Zhang, S. Tao, W. Chu, Q. Zhang, Y. Luo, C. Wu, Y. Xie, *Adv. Mater.* **2016**, *28*, 2427; e) P. Liu, Y. Zhao, R. Qin, S. Mo, G. Chen, L. Gu, D. M. Chevrier, P. Zhang, Q. Guo, D. Zang, B. Wu, G. Fu, N. Zheng, *Science* **2016**, *352*, 797; f) X. Guo, G. Fang, G. Li, H. Ma, H. Fan, L. Yu, C. Ma, X. Wu, D. Deng, M. Wei, D. Tan, R. Si, S. Zhang, J. Li, L. Sun, Z. Tang, X. Pan, X. Bao, *Science* **2014**, *344*, 616; g) M. Moliner, J. E. Gabay, C. E. Kliewer, R. T. Carr, J. Guzman, G. L. Casty, P. Serna, A. Corma, *J. Am. Chem. Soc.* **2016**, *138*, 15743; h) Y. Chen, S. Ji, Y. Wang, J. Dong, W. Chen, Z. Li, R. Shen, L. Zheng, Z. Zhuang, D. Wang, Y. Li, *Angew. Chem., Int. Ed.* **2017**, *56*, 6937; i) Z. Zhang, Y. Zhu, H. Asakura, B. Zhang, J. Zhang, M. Zhou, Y. Han, T. Tanaka, A. Wang, T. Zhang, N. Yan, *Nat. Commun.* **2017**, *8*, 16100.
- [2] a) M. Moses-DeBusk, M. Yoon, L. F. Allard, D. R. Mullins, Z. Wu, X. Yang, G. Veith, G. M. Stocks, C. K. Narula, *J. Am. Chem. Soc.* **2013**, *135*, 12634; b) T. E. James, S. L. Hemmingson, C. T. Campbell, *ACS Catal.* **2015**, *5*, 5673; c) A. Uzun, V. Ortalan, Y. Hao, N. D. Browning, B. C. Gates, *ACS Nano* **2009**, *3*, 3691; d) K. Ding, A. Gulec, A. M. Johnson, N. M. Schweitzer, G. D. Stucky, L. D. Marks, P. C. Stair, *Science* **2015**, *350*, 189.
- [3] a) J. H. Kwak, J. Hu, D. Mei, C.-W. Yi, D. H. Kim, C. H. F. Peden, L. F. Allard, J. Szanyi, *Science* **2009**, *325*, 1670; b) G. Vilé, D. Albani, M. Nachtegaal, Z. Chen, D. Dontsova, M. Antonietti, N. López, J. Pérez-Ramírez, *Angew. Chem., Int. Ed.* **2015**, *54*, 11265; c) B. Zhang, H. Asakura, J. Zhang, J. Zhang, S. De, N. Yan, *Angew. Chem., Int. Ed.* **2016**, *55*, 8319.
- [4] a) H.-C. Zhou, J. R. Long, O. M. Yaghi, *Chem. Rev.* **2012**, *112*, 673; b) H.-C. Zhou, S. Kitagawa, *Chem. Soc. Rev.* **2014**, *43*, 5415; c) T. R. Cook, Y.-R. Zheng, P. J. Stang, *Chem. Rev.* **2013**, *113*, 734; d) Q.-L. Zhu, Q. Xu, *Chem. Soc. Rev.* **2014**, *43*, 5468; e) Z. Fang, B. Bueken, D. E. D. Vos, R. A. Fischer, *Angew. Chem., Int. Ed.* **2015**, *54*, 7234; f) T. Islamoglu, S. Goswami, Z. Li, A. J. Howarth, O. K. Farha, J. T. Hupp, *Acc. Chem. Res.* **2017**, *50*, 805; g) B. Li, H.-M. Wen, Y. Cui, W. Zhou, G. Qian, B. Chen, *Adv. Mater.* **2016**, *28*, 8819.
- [5] a) Q. Yang, Q. Xu, H.-L. Jiang, *Chem. Soc. Rev.* **2017**, *46*, 4774; b) H. R. Moon, D.-W. Lim, M. P. Suh, *Chem. Soc. Rev.* **2013**, *42*, 1807; c) A. Aijaz, A. Karkamkar, Y. J. Choi, N. Tsumori, E. Rönnebro, T. Autrey, H. Shioyama, Q. Xu, *J. Am. Chem. Soc.* **2012**, *134*, 13926; d) S. Li, F. Huo, *Nanoscale* **2015**, *7*, 7482; e) H. Liu, L. Chang, C. Bai, L. Chen, R. Luque, Y. Li, *Angew. Chem., Int. Ed.* **2016**, *55*, 5019; f) P. Hu, J. V. Morabito, C.-K. Tsung, *ACS Catal.* **2014**, *4*, 4409; g) X. Li, T. W. Goh, L. Li, C. Xiao, Z. Guo, X. C. Zeng, W. Huang, *ACS Catal.* **2016**, *6*, 3461; h) M. Zhao, K. Yuan, Y. Wang, G. Li, J. Guo, L. Gu, W. Hu, H. Zhao, Z. Tang, *Nature* **2016**, *539*, 76.
- [6] a) P. Ji, K. Manna, Z. Lin, X. Feng, A. Urban, Y. Song, W. Lin, *J. Am. Chem. Soc.* **2017**, *139*, 7004; b) Z. Li, N. M. Schweitzer, A. B. League, V. Bernales, A. W. Peters, A. B. Getsoian, T. C. Wang, J. T. Miller, A. Vjunov, J. L. Fulton, J. A. Lercher, C. J. Cramer, L. Gagliardi, J. T. Hupp, O. K. Farha, *J. Am. Chem. Soc.* **2016**, *138*, 1977.
- [7] a) K. Manna, T. Zhang, W. Lin, *J. Am. Chem. Soc.* **2014**, *136*, 6566; b) X. Li, R. V. Zeeland, R. V. Maligal-Ganesh, Y. Pei, G. Power, L. Stanley, W. Huang, *ACS Catal.* **2016**, *6*, 6324; c) A. Fateeva, P. A. Chater, C. P. Ireland, A. A. Tahir, Y. Z. Khimyak, P. V. Wiper, J. R. Darwent, M. J. Rosseinsky, *Angew. Chem., Int. Ed.* **2012**, *51*, 7440; d) N. Kornienko, Y. Zhao, C. S. Kley, C. Zhu, D. Kim, S. Lin, C. J. Chang, O. M. Yaghi, P. Yang, *J. Am. Chem. Soc.* **2015**, *137*, 14129; e) D. Feng, Z.-Y. Gu, J.-R. Li, H.-L. Jiang, Z. Wei, H.-C. Zhou, *Angew. Chem., Int. Ed.* **2012**, *51*, 10307.
- [8] a) Y. Fu, D. Sun, Y. Chen, R. Huang, Z. Ding, X. Fu, Z. Li, *Angew. Chem., Int. Ed.* **2012**, *51*, 3364; b) H.-Q. Xu, J. Hu, D. Wang, Z. Li, Q. Zhang, Y. Luo, S.-H. Yu, H.-L. Jiang, *J. Am. Chem. Soc.* **2015**, *137*, 13440; c) J.-D. Xiao, Q. Shang, Y. Xiong, Q. Zhang, Y. Luo, S.-H. Yu, H.-L. Jiang, *Angew. Chem., Int. Ed.* **2016**, *55*, 9389; d) H. Zhang, J. Wei, J. Dong, G. Liu, L. Shi, P. An, G. Zhao, J. Kong, X. Wang, X. Meng, J. Zhang, J. Ye, *Angew. Chem., Int. Ed.* **2016**, *55*, 14310; e) K. M. Choi, D. Kim, B. Rungtaweivoranit, C. A. Trickett, J. T. D. Barmanbek, A. S. Alshammari, P. Yang, O. M. Yaghi, *J. Am. Chem. Soc.* **2017**, *139*, 356; f) S. Wang, X. Wang, *Small* **2015**, *11*, 3097; g) A. Dhakshinamoorthy, A. M. Asiri, H. García, *Angew. Chem., Int. Ed.* **2016**, *55*, 5414; h) T. Zhang, W. Lin, *Chem. Soc. Rev.* **2014**, *43*, 5982; i) Y. Horiuchi, T. Toyao, M. Saito, K. Mochizuki, M. Iwata, H. Higashimura, M. Anpo, M. Matsuoka, *J. Phys. Chem. C* **2012**, *116*, 20848; j) S. Pullen, H. Fei, A. Orthaber, S. M. Cohen, S. Ott, *J. Am. Chem. Soc.* **2013**, *135*, 16997; k) T. Zhou, Y. Du, A. Borgna, J. Hong, Y. Wang, J. Han, W. Zhang, R. Xu, *Energy Environ. Sci.* **2013**, *6*, 3229; l) K. Sasan, Q. Lin, C. Y. Mao, P. Feng, *Chem. Commun.* **2014**, *50*, 10390.
- [9] a) D. A. Wheeler, J. Z. Zhang, *Adv. Mater.* **2013**, *25*, 2878; b) K. Wu, H. Zhu, T. Lian, *Acc. Chem. Res.* **2015**, *48*, 851; c) F. Lei, L. Zhang, Y. Sun, L. Liang, K. Liu, J. Xu, Q. Zhang, B. Pan, Y. Luo, Y. Xie, *Angew. Chem., Int. Ed.* **2015**, *54*, 9266.
- [10] B. Pattengale, S. Yang, J. Ludwig, Z. Huang, X. Zhang, J. Huang, *J. Am. Chem. Soc.* **2016**, *138*, 8072.
- [11] a) W. Bi, L. Zhang, Z. Sun, X. Li, T. Jin, X. Wu, Q. Zhang, Y. Luo, Y. Wu, Y. Xie, *ACS Catal.* **2016**, *6*, 4253; b) S. Han, Y. Pu, L. Zheng, L. Hu, J. Z. Zhang, X. Fang, *J. Mater. Chem. A* **2016**, *4*, 1078.